



Cite this: DOI: 10.1039/c7ee03397d

The merit of perovskite's dimensionality; can this replace the 3D halide perovskite?

Lioz Etgar 

This perspective paper focuses on the dimensionality of organic–inorganic halide perovskites and their relevant advantages over 3D perovskites. The charges in two-dimensional (2D) materials are restricted in their movement to the two-dimensional plane; however, their confined structure allows one to tune the optical and electronic properties by varying their thickness. Here we focus on the main advantages of 2D halide perovskites including their enhanced stability; several recent reports discussing this point are summarized. It was observed that 2D perovskites exhibit enhanced moisture resistivity, starting from films to complete solar cells. The power conversion efficiency of photovoltaic solar cells based on 2D- and quasi-2D perovskites (2D + 3D perovskites) as light harvesters has been increasing but still not as much as 3D perovskites. However, their other advantages (e.g., stability, tuning of optical and electronic properties, and the large amount of possible organic cations that can be integrated into their structure) make them a stable alternative for efficient and large-scale module solar cells, which may constitute the next step for commercializing perovskite-based solar cells. To sum up, several strategies for improving the photovoltaic performance of low dimensional perovskites are discussed.

Received 29th November 2017,
Accepted 14th December 2017

DOI: 10.1039/c7ee03397d

rsc.li/ees

Broader context

During the past few years, hybrid organic–inorganic perovskites have become one of the most promising materials in the photovoltaic field. In less than five years, the efficiency of perovskite solar cells has quickly increased to 22.1%. The attractive properties of perovskites such as high absorption coefficients, long diffusion lengths, easy processability and extremely low production costs make perovskite solar cells a potential technology for future commercialization for large-scale electricity production. However, the resistivity of perovskites to humidity is still an issue that needs to be solved. Organic–inorganic perovskites contain 3-dimensional arrays of inorganic PbX_6 anions surrounded by organic ammonium counter ions. However, closely related solids exist, based on the same ionic species, which are arranged in 2-dimensional n -lead halide-thick layers separated by sheets of organic cations. Two-dimensional organic–inorganic perovskites are becoming attractive due to their enhanced stability compared to 3D perovskites. This perspective concentrates on the merits of two-dimensional perovskites and their potential to overcome the stability issue of their three-dimensional counterparts, which might open the way for commercialization of this new generation of solar cells.

Introduction

Organic–inorganic perovskites have shown considerably increased potential in recent years by functioning as light harvesters in solar cells. Some of their advantages are that they have a direct band gap, large absorption coefficients,¹ and long diffusion lengths.^{2,3,27}

Several researchers have used $\text{CH}_3\text{NH}_3\text{PbI}_3$ ($\text{CH}_3\text{NH}_3 = \text{MA}$) perovskites as sensitizers in photoelectrochemical cells with liquid electrolytes.^{4–6} However, the performance of these systems has rapidly declined owing to dissolution of the perovskite, which was alleviated by replacing the electrolyte with a solid-state hole conductor.⁷ Owing to intensive work on the perovskite structure,

the solar cell structure, and the deposition techniques (e.g., one-step, two-step deposition, and co-evaporation of perovskite films) for various active layers,^{5,8–19} the efficiency currently reaches approximately 22.1%.²⁰

The operating mechanism underlying these perovskite solar cells has also been investigated using electron beam-induced current (EBIC), Kelvin probe force microscopy (KPFM), and impedance spectroscopy measurements^{21–25} to analyze the solar cell structure, carrier accumulation, and grain boundaries. Modeling of mixed halide perovskites for photovoltaic applications was demonstrated; good agreement was found between the calculated band structures and the experimental trend of optical band gaps.²⁶ In addition, a long-range electron–hole diffusion length was found in organic–inorganic perovskite absorbers, which is one of the main reasons for the high solar cell efficiency.^{27–29}

The Hebrew University of Jerusalem, Institute of Chemistry, Casali Center for Applied Chemistry, Jerusalem, Israel. E-mail: lioz.etgar@mail.huji.ac.il

Several reports have demonstrated the ability to use perovskites as hole conductors in addition to their functionality as light harvesters. For example, power conversion efficiencies as high as 11.2% and 12.8% were achieved for such structures using gold or carbon contacts, respectively.^{30–35}

As mentioned, 3D perovskites have been recognized as promising light harvesters in solar cells; however, their sensitivity to moisture, which requires controllable conditions for their processing, makes it an obstacle for successful commercialization.

Recently, some work has been devoted to implementing two-dimensional perovskites in optoelectronic applications owing to their better resistivity to humidity.³⁶ Smith *et al.* showed the use of phenyl ethylammonium as a barrier for 3 perovskite layers ($n = 3$) having 4.7% efficiency and improved stability.³⁷ Remarkably, Sargent *et al.* demonstrated the use of quasi-2D perovskites in solar cells, achieving a power conversion efficiency of 15.3%. However, the best PV performance was achieved for 60 perovskite layers, which have a longer carrier lifetime than 3D perovskites.³⁸ Kanatzidis *et al.* tuned the number of perovskite layers using butyl ammonium as the barrier. A detailed physical and crystallographic study indicated that perovskite layers grew parallel to the substrate, which hindered them from achieving higher efficiencies.³⁹ Tsai *et al.* used a hot casting deposition technique to ensure that the alignment of the perovskite layers is perpendicular to the substrate. As a result, 4-layered perovskites with butyl ammonium as the barrier achieved 12.5% efficiency.⁴⁰

This perspective paper describes the properties and the formation of 2D- and quasi-2D halide perovskites. An overview of the stability of 2D halide perovskites for different n values will be presented both for films and for complete photovoltaic cells. Finally, the future outlook of these materials in optoelectronic devices and whether they can serve as a better alternative to 3D perovskites will be discussed.

Structure of organic–inorganic lead halide perovskites and their dimensionality

Organic–inorganic perovskite crystals have the configuration $R_2(\text{CH}_3\text{NH}_3)_{n-1}\text{M}_n\text{X}_{3n+1}$, where R is an organic group, M is a divalent metal in the oxidized state (such as Cu^{2+} , Mn^{2+} , Sn^{2+} , Fe^{2+} , and Pb^{2+}), and X is a halide (Cl^- , Br^- , or I^-).⁴¹

The inorganic layers consist of sheets of corner-sharing metal halide octahedra. The M cation is generally a divalent metal that satisfies charge balancing and adopts octahedral anion coordination.⁴²

The inorganic layers are usually termed perovskite sheets, because they are derived from a three-dimensional AMX_3 perovskite structure (A-cation), by making a one-layer-thick cut along the $\langle 100 \rangle$ direction of the three-dimensional crystal lattice. The structure can be modified by changing the compositions of the organic and inorganic salts in the starting solution to tailor the electronic, optical, and magnetic properties.

The organic component consists of a bilayer or a monolayer of organic cations. With a monolayer (monoammonium, for example), the ammonium head of the cation bonds to the halogens in one inorganic layer, and the organic group extends into the space between the inorganic layers. The organic ammonium groups form a layer with a low dielectric constant of ~ 2.4 , whereas the metal halide layers have a high dielectric constant of more than 6,⁴³ and function as a periodic array of barriers and quantum wells, respectively.

In low-dimensional systems, the stability of excitons in quantum wells is greatly enhanced due to the confinement of attracting quasi-particles. The exciton binding energies of typical 2D organic–inorganic perovskites range up to 300 meV and their self-assembled films exhibit bright photoluminescence at room temperature.⁴⁰ Another interesting feature of perovskites is that they combine the virtues of organic flexibility (in terms of the tunability of their properties and relatively simple processability), inorganic mobility, and robustness in a single material. Furthermore, this family of materials permits the tuning of optical and electrical properties by changing either the organic or inorganic component, or their relative abundance.

Fig. 1 shows the dimensionality of the perovskite structure. Here R is a carbon chain with an ammonium group at the end, which yields compounds with different layer (n) values (*e.g.*, $n = 1$, $n = 2, \dots, n = \infty$). In this way, $n = \infty$ is a cubic 3D perovskite such as $\text{CH}_3\text{NH}_3\text{PbI}_3$, whereas the other n values describe 2D ($n = 1$) or quasi-2D ($n > 1$) perovskite structures.

It is assumed that once methyl ammonium is mixed with a long organic cation (starting from $n = 2$) there is no accurate number of layers in the film. For example, in the case of $n = 3$, there are probably $n = 2$ and $n = 1$ perovskite layers. This can be termed a quasi-2D perovskite (or a 2D + 3D perovskite) since it

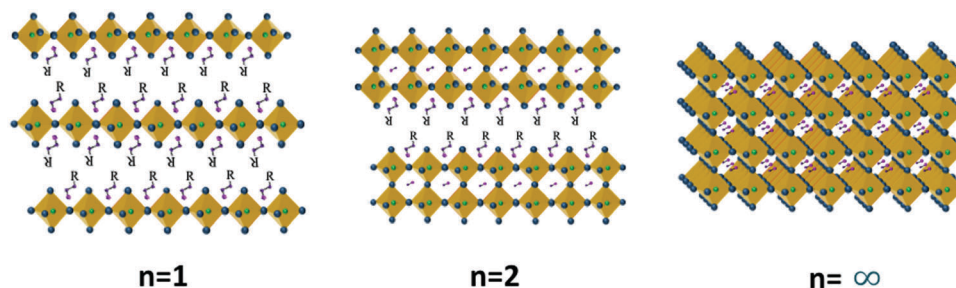


Fig. 1 A scheme showing the evolution of the perovskite dimensionality from $n = 1$, for a 2D perovskite structure, to $n = \infty$ for a 3D perovskite structure. R represents a carbon chain.

is not a pure 2D perovskite. It is important to mention that even in the case of high n values (*i.e.* $n = 40, 50, 60$) the addition of spacer molecules creates layered perovskite structures.

Electronic structure of 2D-layered perovskites

The structure of a 2D-layered perovskite has a unique configuration with interesting physical properties. The 2D-layered perovskite consists of organic layers around 1 nm thick and inorganic sheets around 0.6 nm thick. The energy gap of the organic layers is much higher than the energy gap of the inorganic layers by at least 3 eV.⁴⁴ In the 2D layered perovskite structure the MX_6^{2-} metal halide octahedra are corner sharing and separated by large organic cations that do not fit into the perovskite structure. As mentioned earlier, their dielectric constants are also very different; as a result, the layered perovskite material is configured as a structure with wells and barriers (Fig. 2).

The most common organic cation used in the 2D-layered perovskite is optically inert; therefore, the optical transition energy is mainly determined by the band gap of the wells (inorganic sheets). The depth of the wells is controlled by the M and X species, whereas the M–X bond length controls the width of the wells. In addition, the number of perovskite layers (*i.e.* n values) creates a confinement in the perovskite structure. When moving from pure 3D perovskites to 2D perovskites, the band gap increases. The quantum confinement and the dielectric confinement are also responsible for this increase in the band gap when the dimensionality is reduced. The barrier width is controlled by the organic cation (R). Therefore, it is possible to tune the emission wavelength over a large range from 350 nm to 800 nm by substituting the metal cation M, the halides X, or the organic cations R.^{45,46} With perovskites containing Ge and Sn, the emission is in the infrared range,⁴⁷ whereas for perovskites containing Pb, the emission is in the visible range.

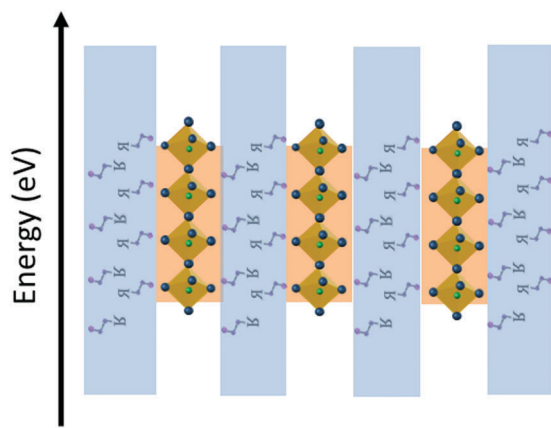


Fig. 2 Quantum well structure of a 2D-layered perovskite. The organic cations function as the barriers, whereas the inorganic framework functions as the well.

Excitons in 2D perovskites

A bound pair of an electron and a hole in the conduction and valence bands, respectively, is called an exciton. Once a material such as a semiconductor absorbs a photon, an exciton is created and electrons and holes attract each other by Coulomb interactions. There are two types of excitons: Wannier–Mott excitons, which are also called free excitons, and Frenkel excitons, which are also called tightly bound excitons. With Wannier–Mott excitons, the dielectric constant is relatively large; as a result, the electric field screening reduces the Coulomb interaction between electrons and holes. Consequently, the exciton binding energy is relatively small. In contrast, in Frenkel excitons the states are localized and tightly bound to specific atoms or molecules. Consequently, the exciton binding energy is relatively large, in the order of 100 meV to ~ 300 meV. The excitons must move through the crystal by hopping or Foerster or Dexter energy transfer from one atom to the other.⁴⁸

In 2D perovskites, the excitons are confined to the inorganic sheets due to the organic barriers. Since the inorganic sheets are very thin (a fraction of nm), the quantum confinement affects the Coulomb interactions between an electron and a hole, which are strongly enhanced in such kinds of molecules. Moreover, the Coulomb interactions in the wells are almost never screened by the presence of the barrier due to the high contrast in the dielectric constants. Consequently, the interaction between an electron and a hole is strengthened, resulting in very large binding energies of several hundreds of meV.^{49,50} With quasi-2D perovskites (*e.g.*, $n = 40, 50, 60, \dots$) the binding energies are smaller, similar to 3D perovskites.³⁷ Therefore it seems that quasi 2D perovskites can function effectively in a photovoltaic cell as the light harvester layer since at room temperature there are free carriers; however, at low n values (*i.e.* $n < 5$) the exciton binding energy is large, as discussed above, and the perovskites have difficulties in functioning in a PV cell, unless one can control the direction of the inorganic perovskite framework to be perpendicular to the substrate. Another option would be to design the PV cell as a bulk heterojunction type solar cell where the interface between TiO_2 and the perovskite is large to assist the charge carrier separation. Finally, it is worth mentioning that perovskites with low n values can function effectively in LEDs.

Stability of 2D perovskites: films and photovoltaic solar cells

One of the main notable features when examining 2D perovskites and quasi-2D perovskites is their potential to enhance the resistivity of perovskites to humidity. The long organic cation should provide more hydrophobicity to the perovskite structure. Liao *et al.*⁵¹ reported better stability of low-dimensional $\text{BA}_2\text{CsPb}_2\text{I}_7$ ($n = 2$), where BA is butyl ammonium. They showed that the BA spacer positively influences its optical properties and affects its structural and compositional stabilities. Fig. 3a shows the powder XRD of CsPbI_3 , which shows degradation after 30 min. This is also true

with MAPbI₃ (Fig. 3c), on which PbI₂ residue appears after 48 hours. On the other hand, the XRD pattern of BA₂CsPb₂I₇ exhibits superior stability for 30 days under 30% humidity conditions (Fig. 3b and d). Aging of complete solar cells was demonstrated; their PCEs retained 92% of their initial values for 30 days without encapsulation.

Furthermore, the perovskite's crystallinity and stability were studied for low dimensional perovskites (low *n* values) by comparing linear butyl amine and iso-butyl amine.⁵² The iso-butyl amine exhibited better crystallinity, an improved out-of-plane orientation, and increased optical absorption. The configuration of planar solar cells is shown in Fig. 4a, which consists of a low dimensional perovskite where *n* = 4 corresponds to (BA)₂(MA)₃Pb₄I₁₃. The iso-butyl-based cells yielded 8.82% PCE, which is higher than that of the *n*-butyl-based cells. Using the hot casting technique, they were able to achieve a PCE value of 10.63% (Fig. 4b). Fig. 4c shows the external quantum efficiency (EQE) spectra of the iso-butyl-based cells prepared at room temperature and by using the hot casting technique. Storing the samples at 20 °C and at 60% humidity without encapsulation shows that the iso-butyl samples could maintain their initial color after storage for 840 hours, which demonstrates their high stability.

Low dimensional perovskites with low *n* values show better stability than high *n* value perovskites.

As discussed above, the superior stability of films and complete solar cells of perovskites with low *n* values can be

observed; however, their PCEs have still lagged behind those of 3D perovskite based cells.

Despite the enhanced stability of layered perovskites with low *n* values compared to layered perovskites with high *n* values, their PV performance is still lower than 2D + 3D perovskites (high *n* values).

In addition to these reports recently, the mixing of 2D + 3D perovskites was studied by Grancini *et al.*,⁵³ who used (HOOC(CH₂)₄NH₃)₂ (AVA) as the long organic cation (2D + 3D means high *n* values, *i.e.* quasi-2D). The authors used two main solar cell structures. As presented in Fig. 5a, in the carbon-based cell no hole transport material (HTM) is used, and in the mesoporous TiO₂-based cell Spiro-OMETAD is used as the HTM. The HTM-free carbon cell, based on 2D + 3D, exhibited 12.9% efficiency, whereas the standard mesoporous cell exhibited 14.6% efficiency. Fig. 5b shows the IV curve and the statistics of the cells based on spiro, whereas a comparison of the cells' stabilities measured under argon and 45 °C is presented in Fig. 5c for 3D and 2D + 3D perovskites. In addition, the scale-up potential was demonstrated, whereby a 10 × 10 cm² module was fabricated having a PCE value of 11.2% and a stability of 1000 h, with no decrease in the performance measured under controlled conditions.

Another 2D + 3D work with improved stability was reported by Ma *et al.*,⁵⁴ who first deposited a 3D perovskite of the MAPbI_xCl_{3-x} type and then spin-coated various concentrations of cyclopropylammonium iodide (CAI). The CAI deposition

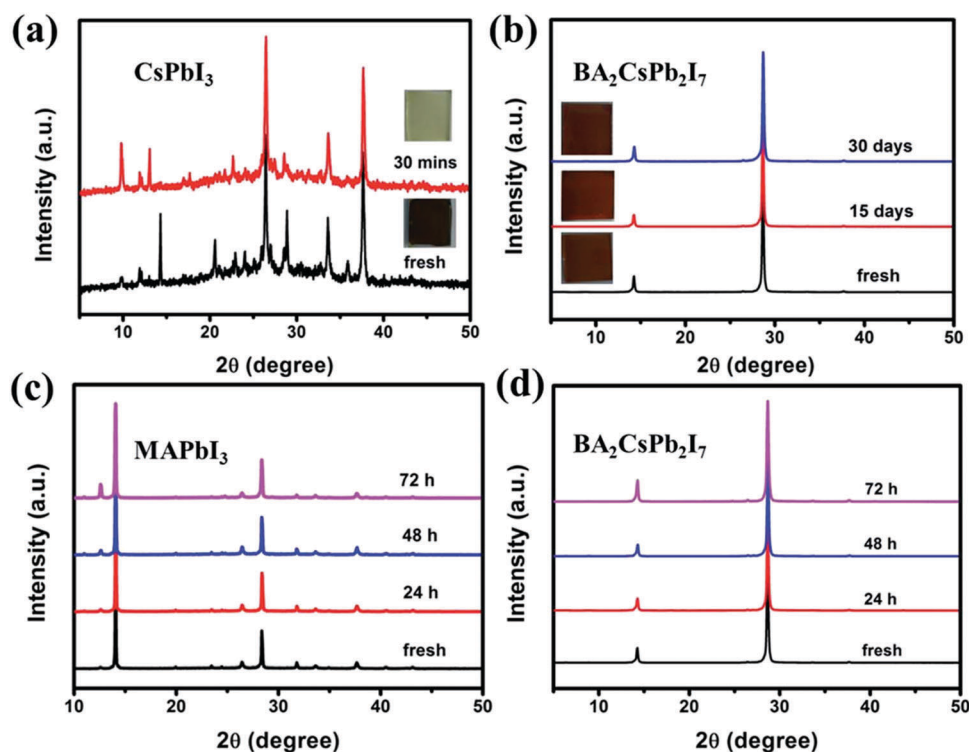


Fig. 3 PXRD patterns of thin films of (a) p-CsPbI₃, (b) BA₂CsPb₂I₇ subjected to 30% relative humidity for different times, (c) MAPbI₃, and (d) BA₂CsPb₂I₇ heated at 85 °C in a glovebox for 3 days. Taken with permission from ref. 51.

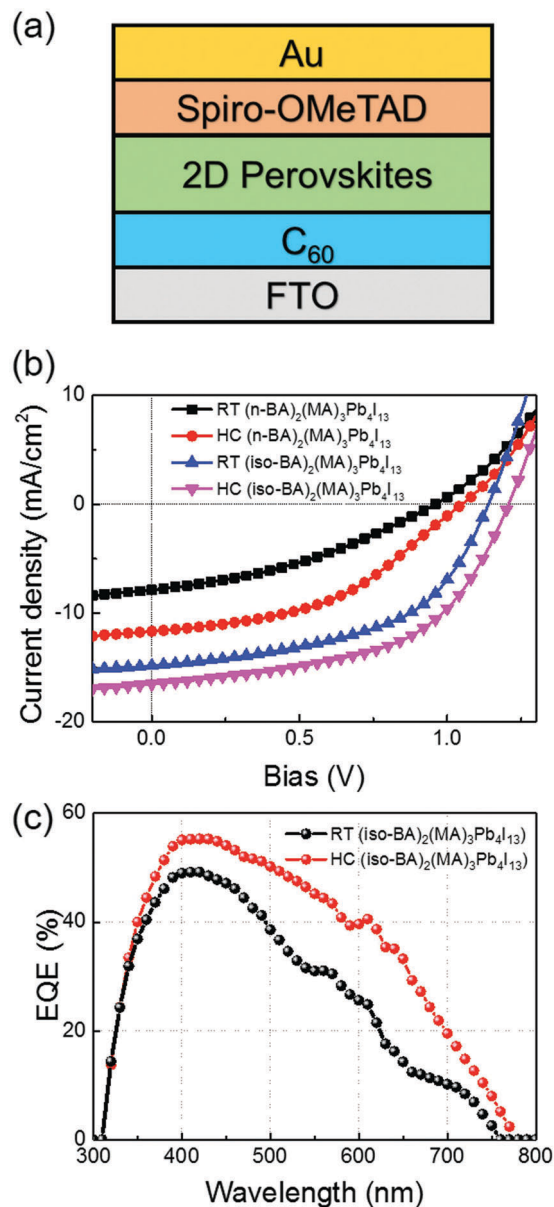


Fig. 4 (a) Schematic depiction of the configuration of an ITO/C60/2D perovskite/spiro-OMeTAD/Au device. (b) Representative current density–voltage (J – V) characteristics of RT and HC fabricated $(n\text{-BA})_2(\text{MA})_3\text{Pb}_4\text{I}_{13}$ and $(\text{iso-BA})_2(\text{MA})_3\text{Pb}_4\text{I}_{13}$ -based solar cells under a light irradiation intensity of 100 mW cm^{-2} in the reverse scan, and (c) EQE spectra of the optimal RT and HC $(\text{iso-BA})_2(\text{MA})_3\text{Pb}_4\text{I}_{13}$ -based solar cells. Taken with permission from ref. 52.

transformed the excess of PbI_2 on the surface to a 2D perovskite having the structure CA_2PbI_4 . This was indicated by XRD and by the increase in the film thickness. It was claimed that CAI just reacts with PbI_2 on the surface and does not penetrate into the 3D perovskite. These 2D + 3D films were stored at an atmospheric humidity of $63 \pm 5\%$. Fig. 6a shows the absorption of the 3D and 2D + 3D films; the 3D perovskite onset diminishes and the PbI_2 characteristic peak appears instead. Eight days later, only the absorption of PbI_2 was observed, which implies the complete decomposition of 3D perovskites. The change in

the film color is shown on the right side of the spectrum. The film color turned from black to yellow (PbI_2) in eight days. On the other hand, the 2D + 3D film survived for a much longer time (40 days) when stored under the same conditions. No change in color was observed for these films, which indicates the enhanced stability of the 2D + 3D perovskite.

An interesting work was performed by synthesizing 2D perovskite compounds using polyethylenimine (PEI) cations within the layered structure. The resulting perovskite is based on the chemical formula $(\text{PEI})_2(\text{MA})_{n-1}\text{Pb}_n\text{I}_{3n+1}$ ($n = 3, 5, 7$).⁵⁵ Photovoltaic solar cells having a large area of 2.32 cm^2 using the PEI were fabricated and compared to 3D cells (Fig. 7A). Fig. 7B shows the dependence of the cell area on the PCE; as can be observed, the PCE value of the 3D cells decreases when the cell area is increased, whereas with the 2D cells it remains constant. Finally, the stability of both large area cells, $(\text{PEI})_2(\text{MA})_6\text{Pb}_7\text{I}_{22}$ and $(\text{PEI})_2(\text{MA})_4\text{Pb}_5\text{I}_{16}$, was good without sealing, whereas their PCE values decreased only by $\sim 5\%$ of their initial values after 500 h light soaking under short-circuit conditions. On the other hand, MAPbI_3 degraded after 5 days by about 50% of its initial PCE value. One more piece of evidence for the better stability of the 2D + 3D perovskite than the 3D perovskite but with comparable PCEs was achieved recently by the addition of *n*-butylammonium cations to a mixed-cation lead mixed-halide $\text{FA}_{0.83}\text{Cs}_{0.17}\text{Pb}(\text{I}_y\text{Br}_{1-y})_3$ 3D perovskite. A stabilized power conversion efficiency of 17.5% was observed. The PCEs of the cells decrease just to 80% of their initial values after 1000 h under 1 Sun illumination for non-encapsulated cells.⁵⁶

The 2D + 3D perovskite (quasi-2D) presents a slightly different direction from that of the low *n* value perovskite; in this case there are mixing of perovskite layers at different *n* values as indicated previously; moreover, the binding exciton energy is the same as that of the 3D perovskite, which makes it attractive for PV cells. Furthermore, the long organic cation added to these structures provides enhanced stability to the films and to complete solar cells.

Addition of 2D perovskites to 3D perovskites stabilizes the perovskite structure and enhances their stability.

It is important to distinguish between thermal and light stability, 2D and 2D + 3D perovskites show better resistivity to humidity compared to other 3D perovskites, inorganic or organic–inorganic; however, we have to take into consideration that when a long organic cation is introduced into the perovskite structure (in order to reduce its dimensionality) its thermal stability reduced. A way to improve this is by using small inorganic cations such as Cs instead of the methylammonium in the 2D or 2D + 3D perovskite. This should improve the thermal stability of the perovskite and possibly provide perovskites with relatively high thermal and light stability.

Summary and outlook

The research and development of 2D halide perovskites as a feasible alternative to 3D-halide perovskites is growing fast. This perspective discusses some of the relevant properties of

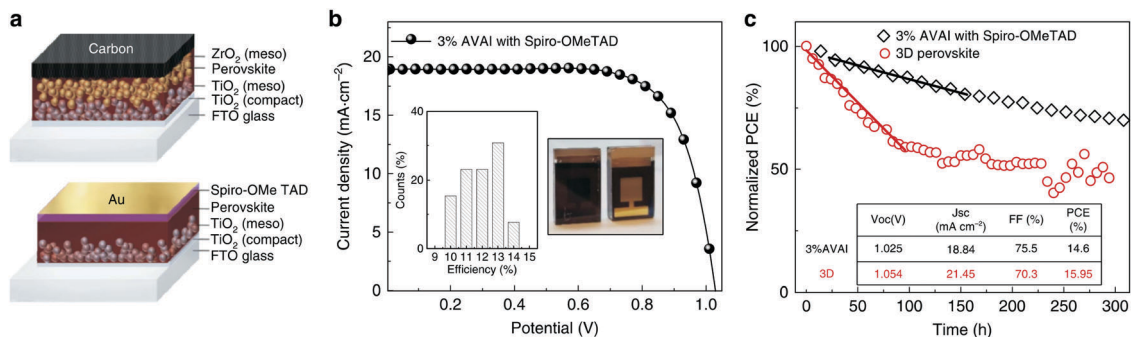


Fig. 5 2D/3D mesoporous solar cell characteristics and stability. (a) Device cartoon of a hole transporting material (HTM)-free solar cell and of a standard HTM-based solar cell. (b) Current density–voltage (J – V) curve using the 2D + 3D perovskite with 3% HOOC(CH₂)₄NH₃l, denoted AVAI hereafter, in a standard mesoporous configuration using 2,2',7,7'-tetrakis(*N,N*-di-*p*-methoxyphenylamine)-9,9'-spirobifluorene (spiro-OMeTAD)/Au (device statistics and a picture of the cell in the inset). (c) Stability curve of the Spiro-OMeTAD/Au cell comparing standard 3D with mixed 2D + 3D perovskites at its maximum power point under AM 1.5G illumination, an argon atmosphere, and a stabilized temperature of 45 °C. The solid line represents the linear fit. In the inset the best device's parameters are listed. Taken with permission from ref. 53.

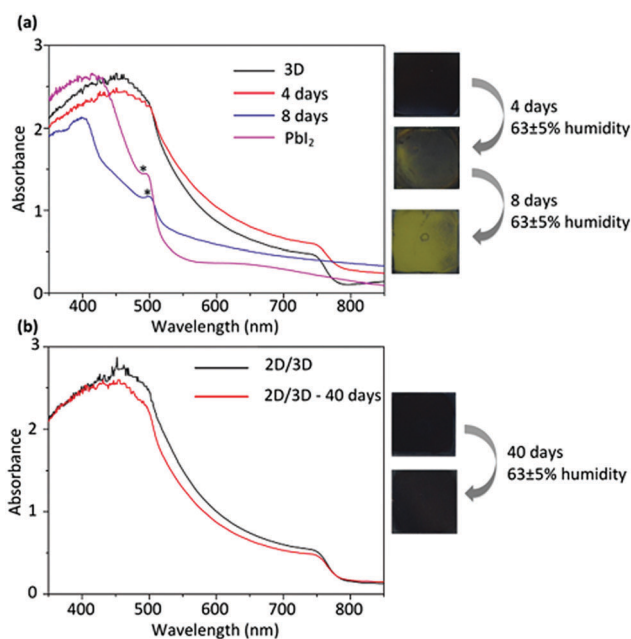


Fig. 6 (a) UV-vis spectra of films of Pbl₂, freshly prepared 3D perovskites, and the same 3D perovskite films after exposure to ambient air for four days and eight days. On the right are images of the 3D perovskite films before and after exposure to ambient air. (b) UV-vis spectra of 2D/3D perovskite hybrid films freshly prepared with 10 mg ml⁻¹ CAI and the same films after exposure to ambient air for 40 days. On the right are images of 2D/3D perovskite hybrid (10 mg ml⁻¹) films before and after exposure to ambient air. Taken with permission from ref. 54.

two-dimensional perovskites, and the electronic structures and excitons in these materials. Moreover, one of the main issues regarding the commercialization of perovskites in optoelectronic devices is their long-term stability. To date, 3D perovskites have exhibited significantly improved performance in PV cells; however, the development of a more stable perovskite is required in order to achieve final products containing it. 2D and quasi-2D perovskites are possible solutions. 2D and quasi-2D perovskites have large organic cations with long alkyl chains which provide

hydrophobicity to the perovskite structure. Therefore, these perovskites have higher resistivity to humidity than 3D perovskites. In this perspective paper we reported recent works on the enhanced stability of 2D and quasi-2D perovskites over 3D perovskites. The power conversion efficiency of 2D perovskites is still not the same as 3D perovskites due to transport problems and the large exciton binding energy; however, recent reports have indicated progress in terms of improvement in the power conversion efficiency of solar cells based on 2D and quasi-2D perovskites.

A way to improve the PV performance in the case of perovskites with low n values is through controlling the direction of the inorganic perovskite framework to be perpendicular to the substrate in order to enhance the transport through selective contacts. In addition, for perovskites with low n values it is suggested that PV cells be designed as bulk heterojunction type solar cells where the interface between the TiO₂ and the perovskite is large enough to assist the charge carrier separation, which is inhibited in low n value perovskites due to their high exciton binding energies. In particular, low n value perovskites are suitable for LED devices due to their high exciton binding energies.

Fig. 8 summarizes several reports on the use of 2D and quasi-2D perovskites in photovoltaic solar cells. This graph presents the power conversion efficiencies of the cells as a function of the n value (the number of layers) of the 2D perovskite and for different organic barrier molecules. In the case of low n values, transport through the perovskite film is inhibited due to the long organic cations; therefore, some directionality of the 2D perovskite on the surface is required in order to achieve high PCE values. With higher n values (*i.e.*, 40, 50, 60), mixing of perovskite layers on the structure occurs, which assists in obtaining better transport properties with the quasi-2D perovskite film; therefore, the directionality is less important. Overall, it can be seen that the PCE values of cells based on 2D and quasi-2D show improvement, which minimizes the drawback of these cells compared with 3D perovskite-based cells. The electronic properties of the 2D perovskite are not necessarily better than the 3D perovskite; however, this could be beneficial in the case of perovskite based solar cells since it might be possible to

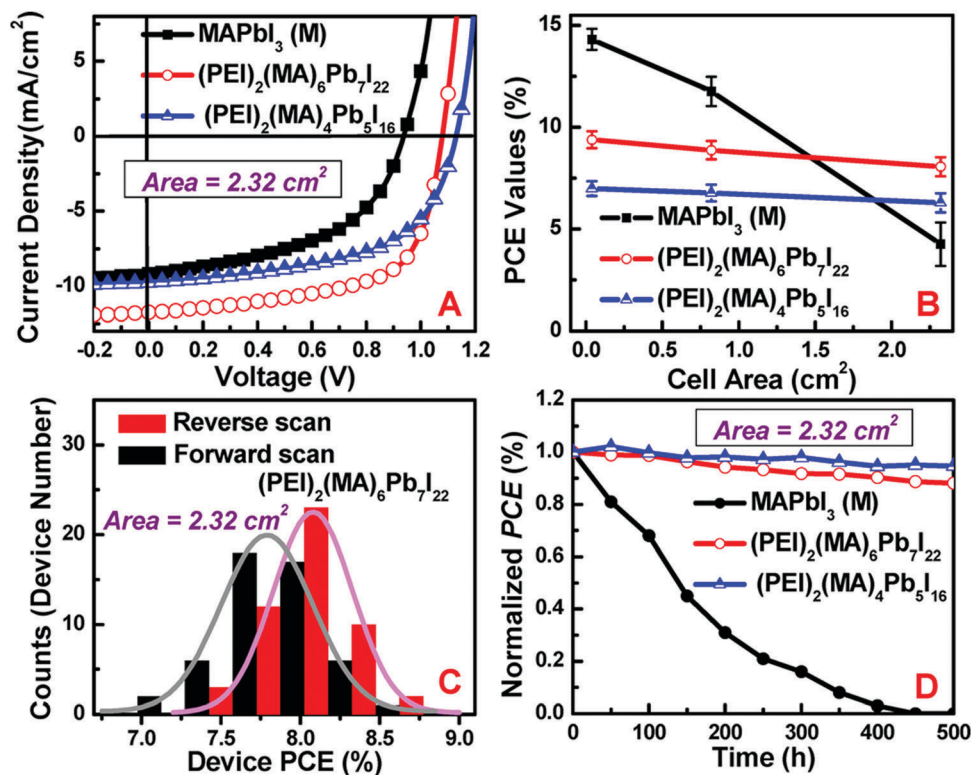


Fig. 7 (A) *J*-*V* curves for the (PEI)₂(MA)_{*n*-1}Pb_{*n*}I_{3*n*+1} perovskites and MAPbI₃ (M)-based devices with an aperture area of 2.32 cm²; (B) graph showing the corresponding PCE value changes of three materials as the device areas change; (C) histogram comparing the differences in the PCEs of large-area solar cells obtained from scanning in the forward and reverse bias directions; and (D) stability of unsealed cells under simulated solar light (AM 1.5; 100 mW cm⁻²) during a shelf life investigation for 500 h. Taken with permission from ref. 55.

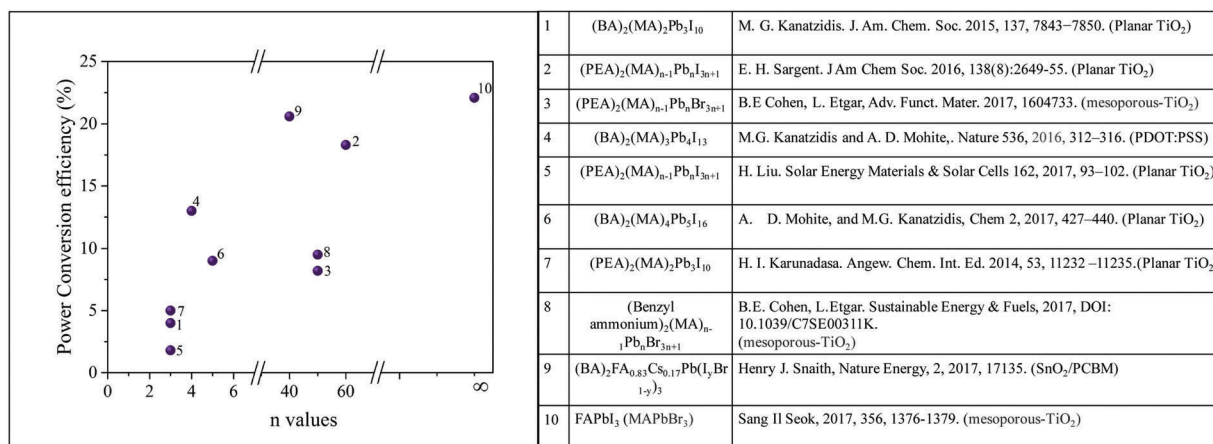


Fig. 8 The efficiency versus the *n* value of selected 2D perovskite-based photovoltaic cells using different barrier molecules. The solar cell bottom layer is indicated. BA, butyl amine; PEA, phenylethylamine.

tune the conductivity through the perovskite structure using different organic cations which can inhibit or enhance the electrical conductivity of the perovskite. For example, the perovskite structure can be designed electronically to be fitted to the selective contacts of the solar cell. The outcome of this will be a low rate of recombination in the solar cell.

Another interesting feature of these 2D and quasi-2D perovskites is the higher open circuit voltage observed in these cells compared

with 3D-based cells, which might be due to lower recombination in this perovskite structure compared with the 3D structure. Fig. 9 shows electron lifetime measurements of quasi-2D perovskites in comparison to 3D perovskites. As can be seen, the electron's lifetime is prolonged with quasi-2D compared with 3D perovskites, an important aspect that should be taken into consideration. In addition to the use of 2D and quasi-2D perovskites in photovoltaic solar cells, there are reports on the use of these

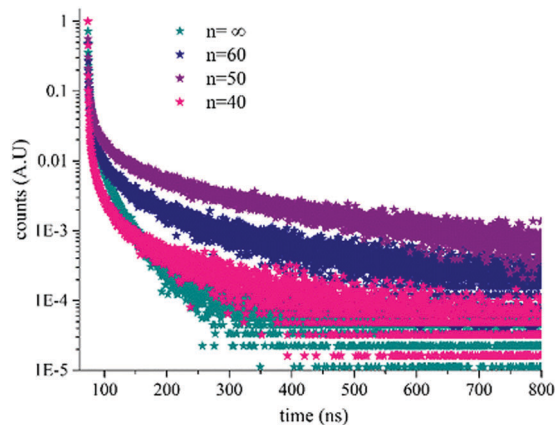


Fig. 9 Electron lifetimes of various n values of quasi-2D bromide perovskites; $n = \infty$ corresponds to 3D perovskites. Taken with permission from ref. 65.

materials in light-emitting diodes as mentioned earlier and photodetectors.^{57–64}

2D and 2D/3D perovskites generate higher open circuit voltages than 3D perovskites.

Overall, the dimensionality of perovskites opens up a whole batch of new materials. The flexibility of choosing the organic cation, having an aromatic ring, a double bond, a long alkyl chain or a cyclo ring, in addition to the tunability of the electrical and optical properties by varying the number of layers (n values) makes these materials very attractive for optoelectronic applications. The choice of an organic cation with an aromatic ring or a double bond could enhance transport through the perovskite structure, while a cation with a long alkyl chain could enhance the resistivity of the perovskite to humidity. Moreover, the optical properties (e.g. band gap) can be tuned by changing the X–Pb–X angle; this can be done by choosing barrier molecules with two amine groups or with long alkyl chains that increase the van der Waals interaction with another barrier molecule. As a result, the X–Pb–X angle could be changed. In contrast, 3D perovskites are much more stringent in terms of using very limited organic cations that can fit into their octahedral cage.

However, to date, 3D perovskites still have several advantages; for example, their exciton binding energies are smaller and currently their PCEs are higher. Applications that use perovskites in their low dimensions are evolving. In addition to the enhanced stability of these materials, the low dimension might be the next step toward commercializing perovskites in optoelectronic applications.

Conflicts of interest

There are no conflicts to declare.

References

1 J. M. Ball, M. M. Lee, A. Hey and H. J. Snaith, *Energy Environ. Sci.*, 2013, **6**, 1739.

2 J. H. Heo, S. H. Im, J. H. Noh, T. N. Mandal, C.-S. Lim, J. A. Chang, Y. H. Lee, H.-j. Kim, A. Sarkar, M. K. Nazeeruddin, M. Grätzel and S. I. Seok, *Nat. Photonics*, 2013, **7**, 486–491.

3 Z. Xiao, C. Bi, Y. Shao, Q. Dong, Q. Wang, Y. Yuan, C. Wang, Y. Gao and J. Huang, *Energy Environ. Sci.*, 2014, **7**, 2619–2623.

4 A. Kojima, K. Teshima, Y. Shirai and T. Miyasaka, *J. Am. Chem. Soc.*, 2009, **131**, 6050–6051.

5 J.-H. Im, J. Chung, S.-J. Kim and N.-G. Park, *Nanoscale Res. Lett.*, 2012, **7**, 353.

6 J.-H. Im, C.-R. Lee, J.-W. Lee, S.-W. Park and N.-G. Park, *Nanoscale*, 2011, **3**, 4088.

7 I. Chung, B. Lee, J. He, R. P. H. Chang and M. G. Kanatzidis, *Nature*, 2012, **485**, 486–489.

8 Y. Wu, X. Yang, H. Chen, K. Zhang, C. Qin, J. Liu and W. Peng, *Appl. Phys. Express*, 2014, **7**, 052301.

9 Z. Xiao, C. Bi, Y. Shao, Q. Dong, Q. Wang, Y. Yuan, C. Wang, Y. Gao and J. Huang, *Energy Environ. Sci.*, 2014, **7**, 2619–2623.

10 A. Abate, M. Saliba, D. J. Hollman, S. D. Stranks, K. Wojciechowski, R. Avolio, G. Grancini, A. Petrozza and H. J. Snaith, *Nano Lett.*, 2014, **14**(6), 3247–3254, DOI: 10.1021/nl500627x.

11 D. Bi, S. J. Moon, L. Haggman, G. Boschloo, L. Yang, E. M. J. Johansson, M. K. Nazeerudin and M. Grätzel, *RSC Adv.*, 2013, **3**, 18762–18766.

12 G. E. Epron, V. M. Burlakov, A. Goriely and H. J. Snaith, *ACS Nano*, 2014, **8**(1), 591–598.

13 G. E. Epron, V. M. Burlakov, P. Docampo, A. Goriely and H. J. Snaith, *Adv. Funct. Mater.*, 2014, **24**, 151–157.

14 J. H. Noh, S. H. Im, J. H. Heo, T. N. Mandal and S. I. Seok, *Nano Lett.*, 2013, **13**, 1764–1769.

15 J. Qiu, Y. Qiu, K. Yan, M. Zhong, C. Mu, H. Yan and S. Yang, *Nanoscale*, 2013, **5**, 3245–3248.

16 J. Burschka, N. Pellet, S.-J. Moon, R. Humphry-Baker, P. Gao, M. K. Nazeeruddin and M. Grätzel, *Nature*, 2013, **499**, 316.

17 M. Liu, M. B. Johnston and H. J. Snaith, *Nature*, 2013, **501**, 395–398.

18 C. Zuo and L. Ding, *Nanoscale*, 2014, **6**, 9935.

19 H. Chen, X. Pan, W. Liu, M. Cai, D. X. Kou, Z. Huo, X. Fang and S. Dai, *Chem. Commun.*, 2013, **49**, 7277–7279.

20 W. S. Yang, B.-W. Park, E. H. Jung, N. J. Jeon, Y. C. Kim, D. U. Lee, S. S. Shin, J. Seo, E. K. Kim, J. H. Noh and S. I. Seok, *Science*, 2017, **356**, 1376–1379.

21 E. Eran, S. Kirmayer, S. Mukhopadhyay, K. Gartsman, G. Hodes and D. Cahen, *Nat. Commun.*, 2014, **5**, 3461.

22 H.-S. Kim, I. Mora-Sero, V. Gonzalez-Pedro, F. Fabregat-Santiago, E. J. Juarez-Perez, N.-G. Park and J. Bisquert, *Nat. Commun.*, 2013, **4**, 2242.

23 Q. Peng, A. L. Domanski, A. K. Chandiran, R. Berger, H.-J. Butt, M. I. Dar, T. Moehl, N. Tetreault, P. Gao, S. Ahmad, M. K. Nazeeruddin and M. Grätzel, *Nanoscale*, 2014, **6**, 1508.

24 E. Edri, S. Kirmayer, A. Henning, S. Mukhopadhyay, K. Gartsman, Y. Rosenwaks, G. Hodes and D. Cahen, *Nano Lett.*, 2014, **14**, 1000–1004.

25 V. W. Bergmann, S. A. L. Weber, F. Javier Ramos, M. K. Nazeeruddin, M. Grätzel, D. Li, A. L. Domanski, I. L. W. S. Ahmad and R. Berger, *Nat. Commun.*, 2014, **5**, 5001.

- 26 E. Mosconi, A. Amat, M. K. Nazeeruddin, M. Grätzel and F. De Angelis, *J. Phys. Chem. C*, 2013, **117**, 13902–13913.
- 27 S. D. Stranks, G. E. Eperon, G. Grancini, C. Menelaou, M. J. P. Alcocer, T. Leijtens, L. M. Herz, A. Petrozza and H. J. Snaith, *Science*, 2013, **342**, 341.
- 28 G. Xing, N. Mathews, S. Sun, S. S. Lim, Y. M. Lam, M. Grätzel, S. Mhaisalkar and T. C. Sum, *Science*, 2013, **342**, 344.
- 29 P. P. Boix, S. Agarwala, T. M. Koh, N. Mathews and S. G. Mhaisalkar, *J. Phys. Chem. Lett.*, 2015, **6**, 898–907.
- 30 W. A. Laben and L. Etgar, *Energy Environ. Sci.*, 2013, **6**, 3249–3253.
- 31 S. Aharon, B. E. Cohen and L. Etgar, *J. Phys. Chem. C*, 2014, **118**, 17160–17165.
- 32 B. E. Cohen, S. Gamliel and L. Etgar, *APL Mater.*, 2014, **2**, 081502.
- 33 J. Shi, J. Dong, S. Lv, Y. Xu, L. Zhu, J. Xiao, X. Xu, H. Wu, D. Li and Q. Meng, *Appl. Phys. Lett.*, 2014, **104**, 063901.
- 34 A. Mei, X. Li, L. Liu, Z. Ku, T. Liu, Y. Rong, M. Xu, M. Hu, J. Chen, Y. Yang, M. Grätzel and H. Han, *Science*, 2014, **345**(6194), 295–298.
- 35 L. Etgar, P. Gao, Z. Xue, Q. Peng, A. K. Chandiran, B. Liu, M. K. Nazeeruddin and M. Grätzel, *J. Am. Chem. Soc.*, 2012, **134**, 17396–17399.
- 36 M. I. Saidaminov, O. F. Mohammed and O. M. Bakr, *ACS Energy Lett.*, 2017, **2**(4), 889–896.
- 37 I. C. Smith, E. T. Hoke, D. Solis-Ibarra, M. D. McGehee and H. I. Karunadasa, *Angew. Chem., Int. Ed.*, 2014, **53**, 11232–11235.
- 38 L. N. Quan, M. Yuan, R. Comin, O. Voznyy, E. M. Beauregard, S. Hoogland, A. Buin, A. R. Kirmani, K. Zhao, A. Amassian, D. H. Kim and E. H. Sargent, *J. Am. Chem. Soc.*, 2016, **138**(8), 2649–2655.
- 39 D. H. Cao, C. C. Stoumpos, O. K. Farha, J. T. Hupp and M. G. Kanatzidis, *J. Am. Chem. Soc.*, 2015, **137**, 7843–7850.
- 40 H. Tsai, W. Nie, J.-C. Blancon, C. C. Stoumpos, R. Asadpour, B. Harutyunyan, A. J. Neukirch, R. Verduzco, J. J. Crochet, S. Tretiak, L. Pedesseau, J. Even, M. A. Alam, G. Gupta, J. Lou, P. M. Ajayan, M. J. Bedzyk, M. G. Kanatzidis and A. D. Mohite, *Nature*, 2016, **536**, 312.
- 41 D. B. Mitzi, Synthesis, *Progress in Inorganic Chemistry*, John Wiley & Sons, Inc., New York, 1999, vol. 48, p. 1.
- 42 D. B. Mitzi, *Inorg. Chem.*, 2000, **39**, 6107.
- 43 X. Hong, T. Ishihara and A. V. Nurmikko, *Phys. Rev. B: Condens. Matter Mater. Phys.*, 1992, **45**, 6961–6964.
- 44 K. Tanaka, F. Sano, T. Takahashi, T. Kondo, R. Ito and K. Ema, *Solid State Commun.*, 2002, **122**, 249–252.
- 45 G. C. Papavassiliou and I. B. Koutselas, *Synth. Met.*, 1995, **71**, 1713–1714.
- 46 D. B. Mitzi, Synthesis, *Progress In Inorganic Chemistry*, John Wiley & Sons, 1999, ch. 1, vol. 48, pp. 1–122.
- 47 C. C. Stoumpos, C. D. Malliakas and M. G. Kanatzidis, *Inorg. Chem.*, 2013, **52**, 9019–9038.
- 48 M. Fox, *Optical Properties of Solids*, Oxford University Press, New York, 2001.
- 49 T. Ishihara, X. Hong, J. Ding and A. V. Nurmikko, *Surf. Sci.*, 1992, **267**, 323–326.
- 50 X. Hong, T. Ishihara and A. V. Nurmikko, *Phys. Rev. B: Condens. Matter Mater. Phys.*, 1992, **45**(12), 6961–6964.
- 51 J.-F. Liao, H.-S. Rao, B.-X. Chen, D.-B. Kuang and C.-Y. Su, *J. Mater. Chem. A*, 2017, **5**, 2066.
- 52 Y. Chen, Y. Sun, J. Peng, W. Zhang, X. Su, K. Zheng, T. Pullerits and Z. Liang, *Adv. Energy Mater.*, 2017, 1700162.
- 53 G. Grancini, C. Roldán-Carmona, I. Zimmermann, E. Mosconi, X. Lee, D. Martineau, S. Narbey, F. Oswald, F. De Angelis, M. Grätzel and M. K. Nazeeruddin, *Nat. Commun.*, 2017, **8**, 15684.
- 54 C. Ma, C. Leng, Y. Ji, A. X. Wei, A. K. Sun, L. Tang, J. Yang, W. Luo, C. Li, Y. Deng, S. Feng, J. Shen, S. Lu, C. Du and H. Shi, *Nanoscale*, 2016, **8**, 18309.
- 55 K. Yao, X. Wang, Y.-X. Xu, F. Li, L. Zhou and M. Perovskite, *Chem. Mater.*, 2016, **28**, 3131–3138.
- 56 Z. Wang, Q. Lin, F. P. Chmiel, N. Sakai, L. M. Herz and H. J. Snaith, *Nat. Energy*, 2017, **2**, 17135.
- 57 T. Hattori, T. Taira, M. Era, T. Tsutsui and S. Saito, *Chem. Phys. Lett.*, 1996, **254**, 103–108.
- 58 R. Li, C. Yi, R. Ge, W. Zou, L. Cheng, N. Wang, J. Wang and W. Huang, *Appl. Phys. Lett.*, 2016, **109**(1–4), 151101.
- 59 T. Fujita, H. Nakashima, M. Hirasawa and T. Ishihara, *J. Lumin.*, 2000, **847**, 87–89.
- 60 M. Yuan, L. N. Quan, R. Comin, G. Walters, R. Sabatini, O. Voznyy, S. Hoogland, Y. Zhao, E. M. Beauregard, P. Kanjanaboos, Z. Lu, D. H. Kim and E. H. Sargent, *Nat. Nanotechnol.*, 2016, **11**, 872–877.
- 61 Z. Xiao, R. A. Kerner, L. Zhao, N. L. Tran, K. M. Lee, T.-W. Koh, G. D. Scholes and B. P. Rand, *Nat. Photonics*, 2017, **11**, 108–115.
- 62 N. Wang, L. Cheng, R. Ge, S. Zhang, Y. Miao, W. Zou, C. Yi, Y. Sun, Y. Cao, R. Yang, Y. Wei, Q. Guo, Y. Ke, M. Yu, Y. Jin, Y. Liu, Q. Ding, D. Di, L. Yang, G. Xing, H. Tian, C. Jin, F. Gao, R. H. Friend, J. Wang and W. Huang, *Nat. Photonics*, 2016, **10**, 699–704.
- 63 L. N. Quan, Y. Zhao, F. P. García de Arquer, R. Sabatini, G. Walters, O. Voznyy, R. Comin, Y. Li, J. Z. Fan, H. Tan, J. Pan, M. Yuan, O. M. Bakr, Z. Lu, D. H. Kim and E. H. Sargent, *Nano Lett.*, 2017, **17**, 3701–3709.
- 64 P. Li, B. N. Shivnananju, Y. Zhang, S. Li and Q. Bao, *J. Phys. D: Appl. Phys.*, 2017, **50**(1–6), 094002.
- 65 B.-E. Cohen, M. Wierzbowska and L. Etgar, *Adv. Funct. Mater.*, 2017, **27**, 1604733.